JOURNAL OF THERMOPHYSICS AND HEAT TRANSFER
Vol. 8, No. 3, July–Sept. 1994

# Effect of Torsion on Heat Transfer in the Curved Annular Sector Duct

G. Yang* and M. A. Ebadian†
*Florida International University, Miami, Florida 33199*

**The effect of torsion on convective heat transfer in a curved annular sector duct with a finite pitch is numerically studied. Seven parameters are identified as major variables describing the flow pattern. The results indicate that torsion will rotate the temperature contours to one side and distort their symmetry. Increasing the Prandtl number will significantly enhance the effect of torsion on the temperature distribution. The torsion effect may also be considerably enhanced by increasing the curvature, the axial pressure gradient, and decreasing the radius ratio. Furthermore, the predicted results are compared with the experimental data and excellent agreement is achieved.**

## Nomenclature

$b$ = pitch of the helix
$D$ = diameter of helix, m
$De$ = Dean number, $Re\varepsilon^{4/2}$
$D_h$ = hydraulic diameter
$D_p$ = dimensionless pressure gradient, Eq. (11)
$d_h$ = dimensionless hydraulic diameter, $D_h/(2R_o)$
$Nu$ = Nusselt number, Eq. (13)
$Pr$ = Prandtl number
$p$ = dimensionless pressure, $p^*/(\rho\nu^2/R_o^2)$
$p^*$ = dimensional pressure, Pa
$Q$ = function, Eq. (6)
$R_i$ = radius of the duct inner wall, m
$R_o$ = radius of the duct outer wall, m
$Re$ = Reynolds number, Eq. (12)
$r$ = dimensionless radial direction coordinate, $r^*/R_o$
$r_m$ = average dimensionless radius, Table 1
$r^*$ = dimensional radial direction coordinate, m
$r^\#$ = radius ratio, $R_i/R_o$
$S$ = source term, Eq. (17)
$s$ = dimensionless axial coordinate, $s^*/R_o$
$s^*$ = dimensional axial coordinate, m
$T$ = dimensionless temperature, $(T^* - T_w^*)/\{(R_o^2 w_b^*/\nu)[-(dT^*/ds^*)]\}$
$T_b$ = bulk temperature
$T^*$ = dimensional temperature, K
$T_w^*$ = wall temperature
$u, v, w$ = dimensionless velocity components, $u^*R_o/\nu$, $v^*R_o/\nu$, and $w^*R_o/\nu$
$u^*, v^*, w^*$ = dimensional velocity components in the $\theta$, $r$, and $s$ directions, m s$^{-1}$
$w_b$ = dimensionless average axial velocity, Eq. (14)
$w_b^*$ = dimensional average axial velocity, m s$^{-1}$, $w_b\nu/R_o$
$\alpha$ = angle between the sector centerline and the direction normal to the helical axis of the holding pipe
$\beta$ = function, Eq. (7)
$\Gamma$ = coefficient
$\gamma$ = function, Eq. (8)
$\varepsilon$ = dimensionless curvature, $\kappa R_o$
$\eta$ = function, Eq. (9)
$\theta$ = angular coordinate
$\kappa$ = curvature, m$^{-1}$ $(D/2)/(D^2/4 + b^2)$
$\lambda$ = dimensionless pitch, $2b/D$
$\nu$ = kinematic viscosity, m$^2$ s$^{-1}$
$\rho$ = density, kg m$^{-3}$
$\Phi$ = general variable, Eq. (17)
$\Omega$ = sector angle
$\omega$ = function, Eq. (10)

*Superscript*
$G$ = Garimella et al.[1]

## Introduction

DUE to their compact structure and high heat transfer coefficient, coiled annular sector duct heat exchangers are used extensively in the chemical, dairy, HVAC, and food industries.[1] The general subject of flow and heat transfer in a coiled pipe has been examined by numerous authors. Excellent reviews can be found in Refs. 2–6. However, these reviews clearly indicate that some subjects of this study have not been clearly understood. For example, results for the convective heat transfer in the coiled pipe with a finite pitch are lacking in the open literature. It is well known that the pitch of a coiled pipe will create an additional force—torsion—on fluid flow. What kind of role torsion plays on heat transfer in a curved duct is not clear, especially for the annular sector cross section duct. Therefore, the objective of this investigation is to study the effect of torsion on convective heat transfer in an annular sector duct.

In a toroidal pipe (the coiled pipe with a zero pitch), two symmetrical loops of secondary flows are formed due to centrifugal force.[7] Truesdell and Adler[8] were the first to introduce the nonorthogonal coordinate system to study the fluid flow in a helicoidal pipe. They solved the problem numerically and concluded that the friction factor in a toroidal coil (zero pitch) could be extended for a helical coil (finite pitch) simply by substituting the helical number for the Dean number. Manlapaz and Churchill[9] further numerically studied the forced convective heat transfer in a coiled pipe with a finite pitch. Wang[10] solved the same problem theoretically using the nonorthogonal helicoidal coordinate system. He found that in the helicoidal pipe torsion will distort the symmetrical loops of the secondary flow. Murata et al.[11] simplified the Navier-Stokes equation by assuming a small curvature in a nonorthogonal coordinate system. Germano[12] introduced a transformation to render the nonorthogonal coordinate system to

Received July 7, 1993; revision received Dec. 27, 1993; accepted for publication Dec. 30, 1993. 

*Assistant Professor, Department of Mechanical Engineering.
†Professor and Chairman, Department of Mechanical Engineering.

an orthogonal one and found that the effect of torsion on the secondary flow is of the second-order. Kao[13] used Germano's coordinate system to study helicoidal pipe flow in a substantial range of Dean numbers using both perturbation and numerical methods. Germano[14] further used the same coordinate system to solve the secondary flow in a curved duct with an elliptical cross section. Tuttle[15] and Xie[16] tried to resolve the controversy between these researchers by linking Wang's coordinate system with Germano's coordinate system. Chen and Jan[17] solved the same problem by using double series expansion method. Recently, Liu and Masliyah[18] numerically studied the pitch effect on laminar flow in a large range of Dean numbers.

In their application, several annular sector ducts are combined side-by-side to form a circular annular pipe bent in the shape of a coil. Studies of flow and heat transfer behavior for the curved annular duct have been conducted recently.[1,19] From an engineering point of view, it is very difficult to manufacture the curved annular pipe. In an actual annular pipe, some supports must be applied to assure that the inner and outer pipes are concentric to each other, which turns the annular duct into an annular sector duct. Yang and Ebadian[20] recently studied the heat transfer behavior in a curved annular sector duct. Due to neglecting the effect of the pitch of the coil, their results are only valid in some limited cases. On the other hand, Yang et al.[21] also studied the torsion effect on heat transfer in a curved pipe with a circular cross section. They found that although torsion can only slightly reduce the friction coefficient for pipe flow, it may significantly reduce the Nusselt number for the fluid with a large Prandtl number. Previous studies[22-24] indicate that the secondary flow pattern and convective heat transfer strongly depend on the cross-sectional configuration of the duct. The annular sector duct has both convex and concave boundaries, whereas the circular pipe has convex boundaries only. The substantial difference in the heat transfer behavior between the curved duct with an annular sector cross section and that of the circular cross section can be expected due to the difference in the boundaries. Furthermore, the symmetrical center of the annular sector duct may not coincide with the normal direction of the holding pipe, which may create additional complexity. These major differences make the convective heat transfer behavior in an annular sector duct with a finite pitch very different from that of a helicoidal pipe with a circular cross section.

## Governing Equations and Numerical Analysis

For a straight annular sector duct, three geometric parameters are adequate to determine the convective heat transfer behavior in the duct: 1) the sector angle, 2) the Prandtl number, and 3) the inner and outer wall radii. However, for a curved annular sector duct with a finite pitch, three more geometric parameters must be specified: 1) the curvature of the pipe, 2) the pitch of the helix, and 3) the relative location of the sector centerline to the curvature direction of the holding pipe and the flow Reynolds number. Figure 1 illustrates the definition of these parameters and the coordinate system used in this study. $s^*$ indicates the centerline of the holding pipe; $D$ is the diameter of the helix on which $s^*$ is coiled; $b$ is the pitch of the helix; $R_i$ and $R_o$ indicate the radii of the inner and outer walls of the annular duct, respectively; $r^*$ and $\theta$ are the coordinates in the radial and tangential directions; $\alpha$ is the relative location of the curved annular sector centerline to the curvature direction of the holding pipe; and $\Omega$ represents the angle of the annular sector.

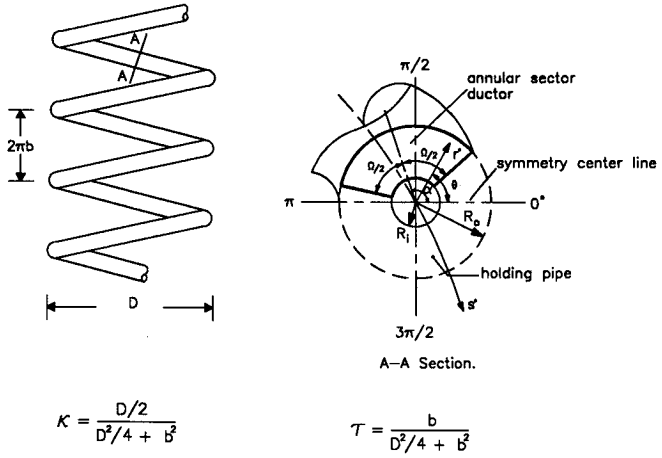


$$K = \frac{D/2}{D^2/4 + b^2} \qquad T = \frac{b}{D^2/4 + b^2}$$

**Fig. 1 Geometry and coordinate system for the curved annular sector duct with considerable pitch.**

The governing equations for the fully developed flow can be written as in Eqs. (1–5) in Germano's coordinate system. The first four equations are basically the same as that of the equation developed by Germano,[12] except they have been rearranged to be convenient for numerical calculation. The energy equation, Eq. (5), is derived in Germano's coordinate system by assuming that the dissipation of flow viscosity is neglected, and a constant wall heat flux axially[21]:

$$\frac{1}{r}\frac{\partial u}{\partial \theta} + \frac{1}{r}\frac{\partial (rv)}{\partial r} + Q = 0 \tag{1}$$

$$\frac{1}{r}\frac{\partial (uu)}{\partial \theta} + \frac{1}{r}\frac{\partial (rvu)}{\partial r} = -\frac{1}{r}\frac{\partial p}{\partial \theta} + \left(\frac{\partial^2 u}{\partial r^2} + \frac{1}{r}\frac{\partial u}{\partial r} + \frac{1}{r^2}\frac{\partial^2 u}{\partial \theta^2}\right) - uQ - \frac{uv}{r} + \varepsilon w\omega\left[w\cos(\theta+\alpha)\frac{\partial u}{\partial \theta}\right] - \left(\frac{1}{r^2}\frac{\partial^2 u}{\partial \theta^2} + \frac{u}{r^2} + \frac{1}{r}\frac{\partial^2 v}{\partial r \partial \theta} - \frac{1}{r^2}\frac{\partial v}{\partial \theta}\right) + \varepsilon\omega\left[\eta\sin(\theta+\alpha) + \lambda\frac{\partial \beta}{\partial \theta}\right] \tag{2}$$

$$\frac{1}{r}\frac{\partial (vu)}{\partial \theta} + \frac{1}{r}\frac{\partial (rvv)}{\partial r} = -\frac{\partial p}{\partial r} + \left(\frac{1}{r^2}\frac{\partial^2 v}{\partial \theta^2} + \frac{1}{r}\frac{\partial v}{\partial r} + \frac{\partial^2 v}{\partial r^2}\right) - vQ + \frac{u^2}{r} + \varepsilon w\omega\left[w\sin(\theta+\alpha) + \lambda\frac{\partial v}{\partial \theta}\right] - \left(\frac{1}{r}\frac{\partial v}{\partial r} + \frac{\partial^2 v}{\partial r^2} + \frac{1}{r}\frac{\partial^2 u}{\partial r \partial \theta} + \frac{1}{r^2}\frac{\partial u}{\partial \theta}\right) - \varepsilon\omega\left[\eta\cos(\theta+\alpha) + \lambda\frac{\partial \gamma}{\partial \theta}\right] \tag{3}$$

$$\frac{1}{r}\frac{\partial (uw)}{\partial \theta} + \frac{1}{r}\frac{\partial (rvw)}{\partial r} = -\omega\frac{D_p}{\sqrt{\varepsilon}} + \omega\varepsilon\frac{\partial p}{\partial \theta} + \left(\frac{1}{r^2}\frac{\partial^2 w}{\partial \theta^2} + \frac{1}{r}\frac{\partial w}{\partial r} + \frac{\partial^2 w}{\partial r^2}\right) - 2wQ + \frac{1}{r}\frac{\partial}{\partial \theta}\left[\varepsilon w\omega\cos(\theta+\alpha) - \varepsilon\omega\lambda\frac{\partial u}{\partial \theta}\right] + \frac{\partial}{\partial r}\left[\varepsilon w\omega\sin(\theta+\alpha) - \omega\varepsilon\lambda\frac{\partial v}{\partial \theta}\right] + \frac{1}{r}\left[\varepsilon w\omega\sin(\theta+\alpha) - \omega\varepsilon\lambda\frac{\partial v}{\partial \theta}\right] \tag{4}$$

$$\frac{1}{r}\frac{\partial (uT)}{\partial \theta} + \frac{1}{r}\frac{\partial (rvT)}{\partial r} = \frac{1}{Pr}\left(\frac{1}{r^2}\frac{\partial^2 T}{\partial \theta^2} + \frac{\partial^2 T}{\partial r^2} + \frac{1}{r}\frac{\partial T}{\partial r}\right) - TQ + \frac{1}{Pr}\varepsilon w\left[\frac{\partial T}{r\partial \theta}\cos(\theta+\alpha) + \frac{\partial T}{\partial r}\sin(\theta+\alpha)\right] + \omega\frac{w}{w_b} + \omega\varepsilon\lambda w\frac{\partial T}{\partial \theta} + \frac{1}{Pr}\omega^2\varepsilon\lambda\frac{\partial}{\partial \theta}\left(\varepsilon\lambda\frac{\partial T}{\partial \theta} - 2\frac{\partial T}{\partial s}\right) \tag{5}$$

The $\varepsilon$ and $\lambda$ represent the dimensionless curvature and pitch, $p$ is the pressure of the fluid, and $Pr$ is the Prandtl number, where

$$Q = \varepsilon\omega\left[u\cos(\theta+\alpha) + v\sin(\theta+\alpha) - \lambda\frac{\partial w}{\partial\theta}\right] \quad (6)$$

$$\beta = \frac{1}{r}\frac{\partial w}{\partial\theta} + \varepsilon\omega\left(w\cos(\theta+\alpha) + \lambda\frac{\partial u}{\partial\theta}\right) \quad (7)$$

$$\gamma = -\frac{\partial w}{\partial r} - \varepsilon\omega\left(w\sin(\theta+\alpha) + \lambda\frac{\partial v}{\partial\theta}\right) \quad (8)$$

$$\eta = \frac{\partial u}{\partial r} + \frac{u}{r} - \frac{1}{r}\frac{\partial v}{\partial\theta} \quad (9)$$

$$\omega = \frac{1}{1+\varepsilon\sin(\theta+\alpha)} \quad (10)$$

$$D_p = \frac{R_o^3}{\nu^2\rho}(\kappa R_o)^{1/2}\frac{dp^*}{ds^*} \quad (11)$$

The dimensionless parameters in Eqs. (1–11) are defined by

$$r = \frac{r^*}{R_o},\quad s = \frac{s^*}{R_o},\quad u = \frac{u^*R_o}{\nu},\quad v = \frac{v^*R_o}{\nu},\quad w = \frac{w^*R_o}{\nu}$$
$$p = p^*/(\rho\nu^2/R_o^2),\quad \varepsilon = \kappa R_o,\quad r^\# = R_i/R_o$$
$$D_h = \frac{2\Omega(R_o^2 - R_i^2)}{2(R_o - R_i) + \Omega(R_o + R_i)} \qquad \Omega < 2\pi$$
$$= 2(R_o - R_i) \qquad \Omega = 2\pi \quad (12)$$
$$d_h = D_h/(2R_o)$$
$$De = Re\varepsilon^{1/2} \qquad Re = \frac{D_h w_b^*}{\nu} = w_b$$
$$T = \frac{T^* - T_w^*}{(R_o^2 w_b^*/\nu)\left[-\dfrac{dT^*}{ds^*}\right]} \qquad \lambda = \frac{2b}{D}$$

In Eq. (12), the superscript (*) indicates the dimensional value.

The Nusselt number is defined by

$$Nu = Prd_h^2/T_b \quad (13)$$

The $w_b$ and $T_b$ are defined by

$$w_b = \frac{1}{\Omega(1 - r^{\#2})}\int_{\alpha-\Omega/2}^{\alpha+\Omega/2}\int_{r^\#}^{1} wr\,dr\,d\theta \quad (14)$$

$$T_b = \frac{1}{\Omega w_b(1 - r^{\#2})}\int_{\alpha-\Omega/2}^{\alpha+\Omega/2}\int_{r^\#}^{1} wTr\,dr\,d\theta \quad (15)$$

$\alpha$ in Eqs. (1–5) is used to consider the different orientations of the duct. $\alpha = 0$ indicates that the duct centerline coincides with the normal direction of the helix holding pipe; $\alpha = (\pi/2)$ indicates the duct centerline is perpendicular to the normal direction, etc. The boundary condition of Eqs. (1–5) are

$$@\ r = r^\# \text{ or } r = 1, \text{ or } \theta = 0, \text{ and } \theta = \Omega$$
$$u = 0,\quad v = 0,\quad w = 0,\quad \text{and}\quad T = 0 \quad (16)$$

## Numerical Analysis

The governing equations, Eqs. (1–5), are nonlinear partial differential equations that can be expressed in the following general form:

$$\frac{1}{r}\frac{\partial(u\Phi)}{\partial\theta} + \frac{1}{r}\frac{\partial(rv\Phi)}{\partial r} = \Gamma\left(\frac{\partial^2\Phi}{\partial r^2} + \frac{1}{r}\frac{\partial\Phi}{\partial r} + \frac{1}{r^2}\frac{\partial^2\Phi}{\partial\theta^2}\right) + S \quad (17)$$

where the general dependent variables, $\Phi = 1, u, v, w$, and $T$, refer to the continuity, momentum, and energy equations, respectively. The SIMPLE algorithm is applied to solve these equations.[25] During the calculation, the following convergence criterion is satisfied for all nodes

$$\frac{\|\Phi_{ij}^{k+1} - \Phi_{ij}^{k}\|}{\|\Phi_{ij}^{k+1}\|} \le 10^{-6} \quad (18)$$

where the superscript $ij$ represents the $\theta$ and $r$ coordinates, and superscript $k$ represents the $k$th iteration. Under-relaxation factors have been applied to obtain a convergent solution. Generally speaking, the greater the Dean number and dimensionless pitch, the smaller the under-relaxation factor. An under-relaxation factor ranging from 0.1 to 0.5 has been used according to different computational circumstances.

To assess the accuracy of the governing equations and the validity of the associated computer program, the predicted results have been compared with the test results from Garimella et al.[1] In their test, an annular duct has been used with inner and outer diameters of 12.7 and 19.74 mm, respectively. $\varepsilon$ and $\lambda$ are 0.0555 and 0.0199, respectively. To ensure the concentricity of the two walls, a spacer wire has been applied between the two walls where it yields an annular sector duct with a $2\pi$ angle. During the test, a constant inner wall temperature and adiabatic outer wall boundary condition have been used. The major parameters and the definitions for the hydraulic diameters, the Reynolds numbers, and the Dean numbers in the Garimella et al.[1] study and this article are listed in Table 1. In order to compare our results with theirs, our Dean numbers and Nusselt numbers have been converted to their definition as

$$De^G = De/1.839 \quad (19)$$

$$Nu^G = \frac{hD_h^G}{k} = \frac{hD_h}{k}\frac{D_h^G}{D_h}$$
$$= Nu\left(\frac{D_h^G}{D_h}\right)\left(\frac{d_i + d_o}{d_i}\right) = 2.327\,Nu \quad (20)$$

Since the Nusselt number defined by Eq. (13) is for the case of a constant temperature for both walls, the term $(d_i + d_o)/d_i$ is used to consider the boundary condition in this case. Figure 2 gives a comparison between the two investigations. The horizontal and vertical coordinates indicate the Dean number and the Nusselt number as defined by Garimella et al.[1] The open squares indicate the test data from Garimella et al.,[1] whereas the two lines in the figure represent our prediction. The solid line indicates the calculation by considering the torsion, and the dot-dash line indicates the prediction when $\lambda = 0$. The figure indicates that the Nusselt number predicted by $\lambda = 0$ is higher than that for the case with torsion, and become lower when $De^G > 500$. It is well known that the critical Reynolds number in a curved pipe will be significantly increased.[26] However, no literature has indicated the critical Reynolds number in a curved annular sector duct. In fact, when $De^G > 500$, the Reynolds number flow reaches 6500, which means the flow may be in a transition region. Therefore, the predicted results beyond $De^G = 500$ are uncertain since the governing equation is formulated for laminar flow. The figure indicates that the prediction when consid-

**Table 1 Major test parameters and their definitions**

| | Present article | Garimella et al.[1] |
|---|---|---|
| Hydraulic diameter | $D_h = 2(r_o - r_i)$ $= 7.04$ mm | $D_h^G = 4[(r_o^2 - r_m^2)/2r_o] = 6.41$ mm $r_m = (r_o + r_i)/2$ |
| Reynolds number | $Re = (w_b D_h/\nu)$ | $Re^G = (w_b D_h^G/\nu) = 0.911Re$ |
| Dean numbers | $De = Re(2r_o/D)^{1/2}$ $= 0.2356Re$ | $De^G = Re^G\left[\frac{(d_o - d_i)}{D}\right]^{1/2}$ $= 0.1407Re^G$ $= 0.495De$ |

$D = 355.6$ mm, $d_i = 12.7$ mm, $d_o = 19.74$ mm, $b = 22.23$ mm, $d_i/d_o = 0.643$, $\varepsilon = 0.0555$, and $\lambda = 0.0199$.

**Table 2 Grid independent test results**

| $L \times M$ | $Nu$ |
|---|---|
| 15 × 15 | 25.78 |
| 20 × 20 | 24.61 |
| 30 × 30 | 24.53 |
| 40 × 40 | 24.53 |
| 60 × 60 | 24.55 |
| 80 × 30 | 24.50 |

$\Omega = 2\pi$, $\alpha = \pi$, $dp/ds = -100{,}000$, $q = 0.1$, $r^\# = 0.3$, and $\lambda = 0.1$.

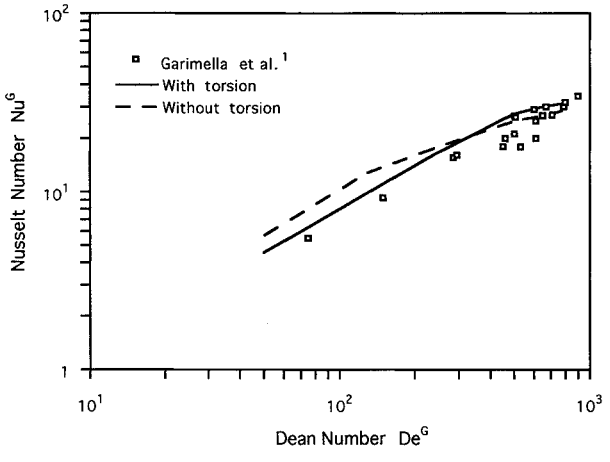


**Fig. 2 Comparison between the present results with the experimental data of Garimella et al.[1]**

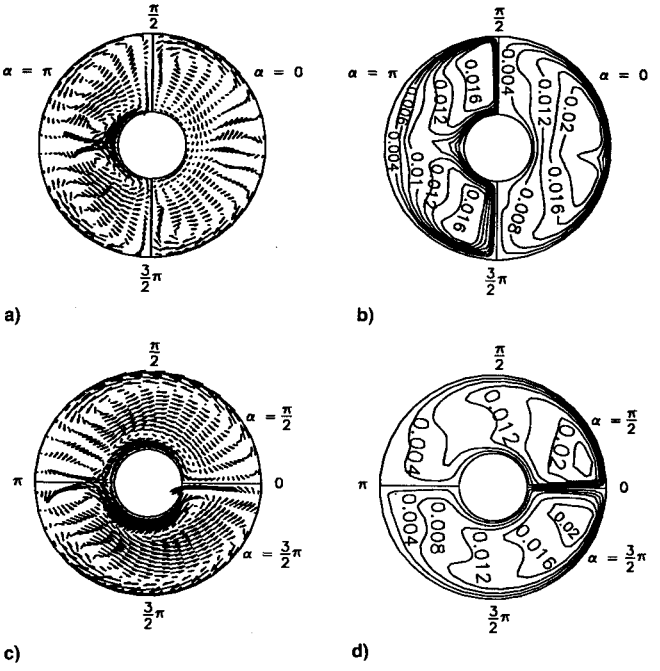


**Fig. 3 Effect of $\alpha$ angle on the flow pattern and temperature distribution ($dp/ds = -100{,}000$, $\varepsilon = 0.2$, $\lambda = 0.05$, $\Omega = \pi$, $r^\# = 0.3$, and $Pr = 0.7$): a) secondary flow pattern and b) temperature distribution in $\alpha = 0$ and $\pi$ ducts; c) secondary flow pattern and d) temperature distribution in $\alpha = \pi/2$ and $3\pi/2$ ducts.**

ering torsion gives us closer results to the experimental data than for the case of not considering the torsion effect.

Numerical experiments have also been conducted to choose independent grids. Since the geometry of the $\Omega = 2\pi$ angle usually requires more grids, this geometry has been applied for this study. Table 2 shows the Nusselt number changes with the grid numbers for the conditions of $\Omega = 2\pi$, $\alpha = \pi$, $dp/ds = -100{,}000$, $\varepsilon = 0.1$, $r^\# = 0.3$, and $\lambda = 0.1$. Grids of 15 × 15, 20 × 20, 30 × 30, 40 × 40, 60 × 60, and 80 × 30 have been tested. The results indicate that a grid of 30 × 30 can provide adequate calculation accuracy. Therefore, all calculations in this study are based on a 30 × 30 grid arrangement.

## Results and Discussion

Since the enhancement of heat transfer in a curved annular sector duct with a finite pitch is strongly dependent on the behavior of the secondary flow, the temperature distribution and the corresponding secondary flow patterns will be discussed simultaneously. Figure 3 indicates the effect of the $\alpha$ angle on the flow pattern and the temperature distribution. As illustrated in Fig. 1, the $\alpha$ angle will determine the location of the annular sector duct relative to the symmetric centerline. It is known that the centrifugal force is directed from the $\pi$ angle to the 0-deg angle along the centerline. A different $\alpha$ angle will therefore change the secondary flow pattern due to the difference in the centrifugal force direction in the duct. In Fig. 3, the flow pattern and temperature distribution in four ducts, when $\alpha = 0$, $\pi/2$, $\pi$, and $3/2\pi$, are presented. In these figures, parameters, $dp/ds = -100{,}000$, $\varepsilon = 0.2$, $\lambda = 0.05$, $\Omega = \pi$, $r^\# = 0.3$, and $Pr = 0.7$, are applied. In Figs. 3a and 3b, the right duct indicates the flow/temperature distributions in the $\alpha = 0$ duct, and the left one is for the $\alpha = \pi$ duct. For the curved annular sector duct without pitch, Yang and Ebadian[20] demonstrated that four vortices exist in both ducts with two vortices in each half-domain symmetric to the centerline, $\pi - 0$ deg. As a result, they indicated that the temperature contours are also symmetric to the centerline. For the $\alpha = 0$ duct, Fig. 3a indicates that torsion has not only distorted the symmetry of the secondary flow, but has also changed the secondary flow structure. A two-vortex flow pattern, instead of four vortices, exists in the $\alpha = 0$ duct. The vortex in the bottom half-domain penetrates to the top half-domain along the outer circular surface, and the one in the top half-domain penetrates down to the bottom domain along the inner circular surface. As a result, Fig. 3b shows the asymmetric temperature distribution in the $\alpha = 0$ duct, with the high temperature contours obviously leaning to the bottom half-domain. Unlike that in the $\alpha = 0$ duct, Fig. 3a shows that the secondary flow in the $\alpha = \pi$ duct is still kept in a four-vortex flow pattern, two near the inner circular surface

**Table 3 Effect of λ on the Nusselt number**

| | *Nu* | | | | |
|---|---|---|---|---|---|
| $\alpha$ | $\lambda = 0$ | 0.05 | 0.1 | 0.15 | 0.2 |
| 0 | 12.42 | 12.40 | 12.31 | 12.09 | 11.90 |
| $\pi/2$ | 13.98 | 13.65 | 13.79 | 13.85 | 13.81 |
| $\pi$ | 14.40 | 14.62 | 14.80 | 14.97 | 14.89 |
| $3/2\pi$ | 13.98 | 14.03 | 14.75 | 15.37 | 16.68 |

$\varepsilon = 0.2$, $\lambda = 0.05$, $\Omega = \pi$, $r^* = 0.3$, $Pr = 0.7$, and $dp/ds = -100{,}000$.

and two near the outer circular surface. However, torsion does distort the symmetry in the secondary flow. Figure 3b shows that two groups of separated eyes exist in both the top and bottom domain. Due to the pitch, the temperature gradient in the top half-domain is much higher than that in the bottom domain. Figures 3c and 3d illustrate the flow pattern and temperature distribution in the $\alpha = \pi/2$ and $\alpha = 3/2\pi$ ducts. In the case of zero torsion, the flow patterns in these two ducts should be identical. Torsion creates a rotational force. As seen in Fig. 3c, the torsion force mainly coincides with the direction of the centrifugal force in the $\alpha = 3/2\pi$ duct, which results in enhancement of the secondary flow. On the other hand, the secondary flow becomes weak in the $\alpha = \pi/2$ duct, due to the torsion force acting against the centrifugal force. Figure 3d illustrates the difference of the temperature contours between the two ducts. It can be seen that torsion significantly changes the temperature gradient near the wall region for both ducts, especially in the regions near the $\pi$ angle. It is known that heat transfer behavior in a duct is mainly dependent on the temperature gradient near the solid wall. Change in the temperature distribution will result in a change in the Nusselt number. Table 3 indicates the effect of torsion on the variation in the Nusselt number for these four ducts. The same parameters have been used as those in Fig. 3, except that the dimensionless pitch changes from 0.05 to 0.2 (corresponding to the $2\pi b/D$ ratio change from 0 to 0.628). For the $\alpha = 0$ duct, the Nusselt number decreases as the torsion increases. When $\lambda$ varies from 0.05 to 0.2, the Nusselt number reduces by about 4%. For the $\alpha = \pi/2$ duct, the Nusselt number does not appear to be sensitive to the change in $\lambda$. Unlike the $\alpha = 0$ duct, the Nusselt number in the $\alpha = \pi$ duct increases as $\lambda$ increases, until $\lambda$ reaches 0.2. The Nusselt number can increase to around 4%. A significant Nusselt number increase can be observed in the $\alpha = 3/2\pi$ duct. For example, for this case, the Nusselt number increases from 13.98 at zero pitch to 16.68 when $\lambda = 0.2$. This is almost a 19% increase, which is contributed by the high-temperature gradient along the solid walls created by the strong secondary flow in this duct, as shown in Fig. 3d.

Figure 4 shows the effect of the radius ratio on the temperature and velocity distributions in the curved annular sector duct with a finite pitch. Parameters of $\alpha = 0$, $\Omega = \pi$, $dp/ds = -100{,}000$, $\varepsilon = 0.1$, $\lambda = 0.1$, and $Pr = 0.7$ have been applied during the calculations. Figures 4a and 4b show the velocity pattern and temperature contours in a $r^* = 0$ duct (semicircular duct). Figure 4a shows that two vortices exist in the $r^* = 0$ duct, although the top one is stronger than the bottom one due to torsion. The asymmetric secondary flow results in the asymmetric temperature gradient, as seen in Fig. 4b. When $r^*$ increases to 0.3, Figs. 4c and 4d show the two asymmetric vortices and the asymmetric temperature distributions. However, when $r^*$ reaches 0.6, a different secondary flow structure exists, two near the inner circular surface, and the other two near the outer circular surface, as seen in Fig. 4e. These four vortices are asymmetrical to the symmetric centerline. Figure 4f shows the corresponding temperature contours in the cross section. This figure illustrates that the high-temperature contours rotate clockwise, which increases the temperature gradient in the bottom half-domain and decreases the temperature gradient in the top half-domain.

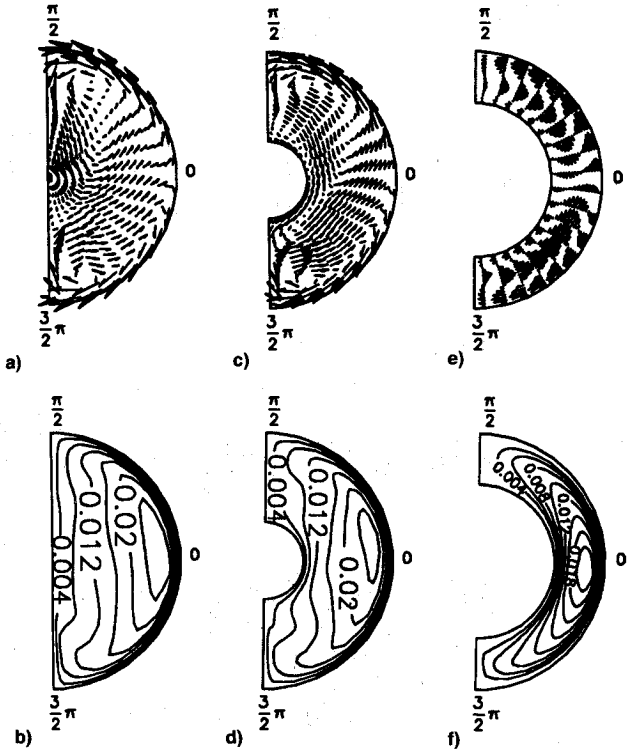


**Fig. 4 Effect of the radius ratio on the temperature and velocity distribution ($dp/ds = -100{,}000$, $\varepsilon = 0.1$, $\lambda = 0.1$, $\Omega = \pi$, $\alpha = 0.0$, and $Pr = 0.7$). Velocity profile for $r^*$ = a) 0.0, c) 0.3, and e) 0.6; temperature distribution for $r^*$ = b) 0.0, d) 0.3, and f) 0.6.**

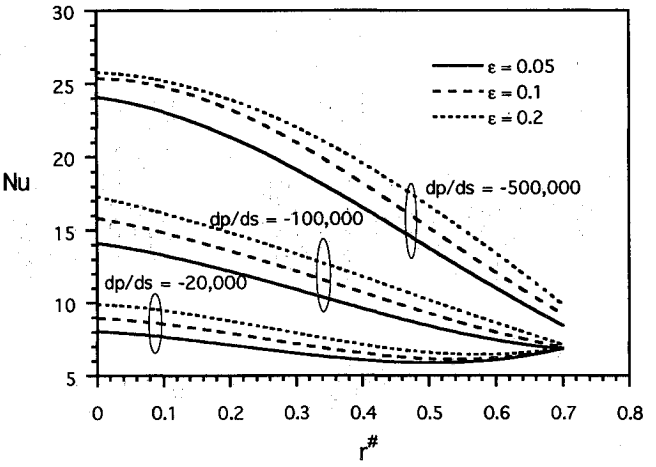


**Fig. 5 Nusselt number variation with the curvature, axial pressure gradient, and radius ratio [$\alpha = 0$, $\Omega = \pi$, and $\lambda = 0.1$].**

Figure 5 shows that the Nusselt number varies with the change in curvature, the axial pressure gradient, and the radius ratio in a helicoidal pipe, where parameters $\alpha = 0$, $\Omega = \pi$, and $\lambda = 0.1$ have been applied. Depending on the axial pressure gradient, the curves have been divided into three groups. The higher the axial pressure gradient, the higher the Nusselt number due to the stronger secondary flow. Generally speaking, at each axial pressure gradient, the Nusselt number increases as $\varepsilon$ increases. At the high and medium axial pressure gradients ($dp/ds = -100{,}000$ and $dp/ds = -20{,}000$), the Nusselt number continuously decreases as the radius ratio increases. However, in the case of a low axial pressure gradient ($dp/ds = -20{,}000$), the Nusselt number decreases as $r^*$ increases at the beginning, after reaching the saddle point around $r^* = 0.5$, and increases again as $r^*$ increases. It is known that the Nusselt number will continuously increase as the radius ratio increases in the straight annular sector duct.[27] In the curved annular sector duct, the secondary flow is in-

duced by the primary flow. At a low axial pressure gradient, the secondary flow becomes very weak in a large radius ratio duct, and enhancement of the heat transfer due to the secondary flow vanishes. This is why the three curves reach almost the same value when $r^* = 0.7$.

The effects of the interaction of the Prandtl number and pitch on the temperature distribution are given in Fig. 6. In this figure, the parameters $\alpha = \pi$, $\Omega = \pi$, $dp/ds = -100{,}000$, $\varepsilon = 0.1$, $r^* = 0.3$ and $\lambda = 0.1$, have been applied. The Prandtl number is the measure of the ratio of convective and diffusive heat transfer. The larger the Prandtl number, the stronger the convective heat transfer. Figure 6a shows the secondary flow pattern for these conditions. Due to the strong right to left directional flow in the center, Fig. 6b shows that the temperature contours are saddled in this region because of the cold fluid penetration. Since pitch exists, the temperature contours are inclined to the top. When the Prandtl number increases from 0.2 to 0.7, the cold fluid penetration becomes even stronger, and the high-temperature contours are divided into two separate islands and the temperature contours become more asymmetric, as seen in Fig. 6c. Figure 6d shows the temperature contours in the case of $Pr = 3$. In this figure, the temperature gradient in the top half-domain is much larger than that in the bottom domain. These figures indicate that the pitch effect on the temperature distribution is significantly enhanced as the Prandtl number increases.

Table 4 shows the Prandtl number effect on the Nusselt number for different annular sector ducts. The parameters of $\alpha = \pi$, $r^* = 0.3$, $dp/ds = -100{,}000$, $\lambda = 0.1$, $\varepsilon = 0.1$ have been applied. Generally speaking, the Nusselt number increases when the fluid Prandtl number increases. When the Prandtl number increases from 0.2 to 5.0, the Nusselt number can increase from 2.5 to 4 times. It is further noted that when the Prandtl number begins to increase, the Nusselt number increases very fast, but when the Prandtl number reaches a certain value, further increase in the Prandtl number can only slightly enhance the Nusselt number.

**Table 4 Effect of the Prandtl number on the Nusselt number in the annular sector duct**

| | *Nu* | | | | |
|---|---|---|---|---|---|
| $\Omega$ | $Pr = 0.2$ | 0.7 | 1.5 | 3.0 | 5.0 |
| $\pi/2$ | 6.886 | 10.74 | 13.93 | 16.94 | 19.83 |
| $\pi$ | 9.445 | 14.73 | 18.90 | 22.16 | 24.52 |
| $\pi$ | 14.81 | 24.61 | 35.77 | 49.31 | 64.53 |

$\varepsilon = 0.1$, $\lambda = 0.1$, $\alpha = \pi$, $r^* = 0.3$, $dp/ds = -100{,}000$, and $Pr = 0.7$.

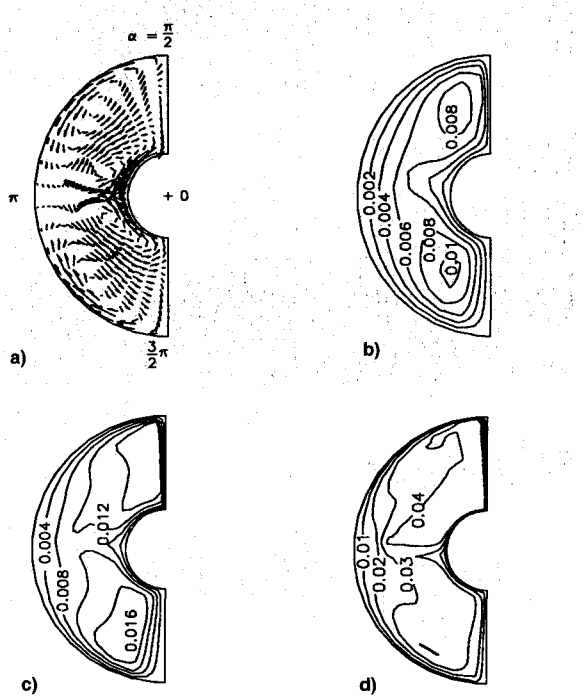


**Fig. 6 Effect of the Prandtl number on the secondary flow and temperature distribution ($dp/ds = -100{,}000$, $\varepsilon = 0.1$, $\lambda = 0.1$, $\Omega = \pi$, $\alpha = \pi$, and $r^* = 0.3$): a) secondary flow; and the temperature distribution for $Pr$ = b) 0.2, c) 0.7, and d) 3.0.**

## Conclusions

The effect of torsion on the convective heat transfer behavior in a curved annular sector duct with a finite pitch has been numerically studied in this article. Seven parameters have been identified as the major variables to determine the behavior of heat transfer. The results are indicated below:

1) Torsion will considerably change the temperature distribution in the annular sector duct. For the $\alpha = 0$ and $\alpha = \pi$ ducts, torsion significantly distorts the symmetry of the temperature contours. For the $\alpha = \pi/2$ and $\alpha = 3/2\pi$ ducts, torsion rotates the temperature contours to one side of the duct.

2) Torsion may increase or decrease the Nusselt numbers, depending on the $\alpha$ angle. For the $\alpha = 0$ and $\alpha = \pi/2$ ducts, increasing torsion will slightly decrease the Nusselt number. However, for the $\alpha = 3/2\pi$ duct, increasing torsion may significantly increase the Nusselt number due to the fact that the torsion force coincides with the direction of the centrifugal force. For example, the Nusselt number will increase 19% when torsion increases from 0 to 0.2 in the $\alpha = 3/2\pi$ duct.

3) The effect of torsion on the temperature distribution is significantly enhanced by increases in the Prandtl number. The high temperature contours become more asymmetric as the Prandtl number increases.

## Acknowledgment

The results presented in this article were sponsored by the National Science Foundation (NSF) under Grant CTS-9017732.

## References

[1]Garimella, S., Chdrards, D. E., and Christensen, R. N., "Experimental Investigation of Heat Transfer in Coiled Annular Ducts," *Journal of Heat Transfer*, Vol. 110, May 1988, pp. 329–336.

[2]Berger, S. A., Talbot, L., and Yao, L. S., "Flow in Curved Pipes," *Annual Review of Fluid Mechanics*, Vol. 15, 1983, pp. 461–512.

[3]Gnielinski, V., "Correlation for the Pressure Drop in Helically Coiled Tubes," *International Chemical Engineering*, Vol. 26, No. 1, 1986, pp. 36–44.

[4]Baurmeister, U., and Brauer, H., "Laminar Flow and Heat Transfer in Helically and Spirally Coiled Tubes," *VDI Forshungsheft*, No. 593, 1979, pp. 2–48.

[5]Nandakumar, K., and Masliyah, J. H., "Swirling Flow and Heat Transfer in Coiled and Twisted Pipes," *Advances in Transport Processes*, Vol. IV, edited by A. S. Mujumdar and R. A. Mashalkar, Wiley Eastern, New York, 1986.

[6]Shah, R. K., and Joshi, S. D., "Convective Heat Transfer in Curved Ducts," *Handbook of Single-Phase Convective Heat Transfer*, edited by S. Kakac, R. K. Shah, and W. Aung, Wiley Interscience, New York, 1987.

[7]Dean, W. R., "Note on the Motion of Fluid in a Curved Pipe," *Philosophy Magazine*, Vol. 4, 1927, pp. 208–223.

[8]Truesdell, L. C., Jr., and Adler, R. J., "Numerical Treatment of Fully Developed Laminar Flow in Helically Coiled Tubes," *American Institute of Chemical Engineering Journal*, Vol. 16, 1970, p. 1010.

[9]Manlapaz, P. L., and Churchill, S. W., "Fully Developed Laminar Convection from a Helical Coil," *Chemical Engineering Communication*, Vol. 9, No. 1, 1981, pp. 185–200.

[10]Wang, C. Y., "On the Low-Reynolds Number Flow in a Helical Pipe," *Journal of Fluid Mechanics*, Vol. 108, 1981, pp. 185–194.

[11]Murata, S., Miyake, T., Inaba, T., and Ogawa, H., "Laminar Flow in a Helically Coiled Pipe," *Bulletin of the Japanese Society of Mechanical Engineering*, Vol. 24, No. 188, 1981, pp. 355–362.

[12]Germano, M., "On the Effect of Torsion in Helical Pipe Flow," *Journal of Fluid Mechanics*, Vol. 125, 1982, pp. 1–8.

[13]Kao, H. C., "Torsion Effect on Fully Developed Flow in a Helical Pipe," *Journal of Fluid Mechanics*, Vol. 184, 1987, pp. 335–356.

[14]Germano, M., "The Dean Equations Extended to Helical Pipe

Flow," *Journal of Fluid Mechanics*, Vol. 203, 1989, pp. 289–356.

[15]Tuttle, E. R., "Laminar Flow in Twisted Pipes," *Journal of Fluid Mechanics*, Vol. 219, 1990, pp. 545–570.

[16]Xie, D. G., "Torsion Effect on Secondary Flow in a Helicoidal Pipe," *International Journal of Heat and Fluid Flow*, Vol. 11, No. 2, 1990, pp. 114–119.

[17]Chen, W. H., and Jan, R., "The Characteristics of Laminar Flow in a Helical Circular Pipe," *Journal of Fluid Mechanics*, Vol. 244, 1992, pp. 241–256.

[18]Liu, S., and Masliyah, J. H., "Axial Invariant Laminar Flow in Helicoidal Pipes with a Finite Pitch," *Journal of Fluid Mechanics*, Vol. 251, 1993, pp. 315–353.

[19]Bharuka, K. S., and Kasture, D. Y., "Flow Through a Helically Coiled Annulus," *Applied Science Research*, Vol. 41, No. 1, 1984, pp. 55–67.

[20]Yang, G., and Ebadian, M. A., "Convective Heat Transfer in a Curved Annular-Sector Duct," *Journal of Thermophysics and Heat Transfer*, Vol. 7, No. 3, 1993, pp. 441–446.

[21]Yang, G., Dong, Z. F., and Ebadian, M. A., "The Effect of Torsion on Convective Heat Transfer in a Helicoidal Pipe Heat Exchanger," *Journal of Heat Transfer*, Vol. 115, No. 4, 1993, pp. 796–800.

[22]Cheng, K. C., and Akiyama, M., "Laminar Forced Convection Heat Transfer in Curved Rectangular Channels," *International Journal of Heat and Mass Transfer*, Vol. 13, No. 3, 1970, pp. 471–490.

[23]Topakoglu, H. C., and Ebadian, M. A., "Viscous Laminar Flow in a Curved Pipe of Elliptical Cross Section," *Journal of Fluid Mechanics*, Vol. 184, 1987, pp. 571–580.

[24]Dong, Z. F., and Ebadian, M. A., "Numerical Analysis of Laminar Flow in the Curved Elliptic Duct," *Journal of Fluid Engineering*, Vol. 113, 1991, pp. 555–562.

[25]Patankar, S. V., *Numerical Heat Transfer and Fluid Flow*, Hemisphere, Washington, DC, 1980.

[26]Srinivasan, P. S., Nandapurkar, S. S., and Holland, F. A., "Friction Factors of Coils," *Transaction of Institute of Chemical Engineering*, Vol. 48, 1970, pp. T156–T161.

[27]Soliman, M. M., "Laminar Heat Transfer in Annular Sector Ducts," *Journal of Heat Transfer*, Vol. 109, No. 1, 1987, pp. 247–269.